STUDIA UNIVERSITATIS BABEŞ-BOLYAI, CHEMIA, XLV, 2, TOM II, 2010

Dedicated to the memory of Prof. dr. Ioan Silaghi-Dumitrescu marking 60 years from his birth

RAMAN IMAGING OF IN VIVO DAMAGED SKIN TISSUES FROM MICE SPECIMENS

ALEXANDRA FALAMAS[a], SIMONA CINTA PINZARU[a,*], CRISTINA A. DEHELEAN[b], MONICA M. VENTER[c]

ABSTRACT Autopsy skin tissues collected from mice specimens exposed to UVB irradiation and 7,12-dimethylbenz(a)anthracene were immersed in formalin solution mixed with colloidal silver nanoparticles and analyzed using Raman imaging. The aim of this study was probe the SERS technique applied to tissue analysis, to detect the main molecular components present in the investigated organs and to search for a new way of acquiring enhanced Raman signal from these tissues for early diagnostic. The analysis of the collected spectra indicated chemisorption of the nanoparticles into the tissue and the possibility to record high quality SERS signal.

Keywords: *Raman imaging, tissue SERS, skin cancer, mouse model, silver nanoparticles*

INTRODUCTION

Raman spectroscopy has currently become a powerful vibrational technique largely used to probe the molecular composition of biological tissues [1-5]. Raman spectra provide information on molecular vibrations leading thus to the possibility of highly specific fingerprinting of the molecular structure and biochemical composition of cells and tissues. In the past two decades there has been a renewed interest in Raman techniques due to the discovery of surface-enhanced Raman scattering (SERS) effect [6-9]. Briefly, the usually weak Raman signals can be greatly enhanced when Raman scattering takes place on molecules at the surface or in very close vicinity to gold or silver nanoparticles. The SERS effect is mainly employed for the investigation of the

[a] *Babes Bolyai University, Dept. of Physics, Kogalniceanu 1, RO 400084, Cluj-Napoca, România*
[b] *Victor Babeş University of Medicine and Pharmacy, Faculty of Pharmacy, Eftimie Murgu Square 2, RO- 300041, Timişoara, România*
[c] *Babes Bolyai University, Faculty of* Chemistry and Chemical Engineering Arany Janos *11, 400028 Cluj-Napoca, Romania*

molecular species adsorbed on noble metal nanoparticles. Recently, SERS was applied in the study of biological cells and tissue [10-12]. Two effects are responsible for this enhancement: the first mechanism is related to resonances between the surface plasmons of the metal nanostructures and the excitation and scattered fields during the Raman process giving rise to enhanced local excitation fields. The second enhancement mechanism is based on the adsorption of the molecules at certain surface sites, creating a charge-transfer state between the metal and the adsorbed scatterer.

SERS in conjunction with Raman imaging technique was applied in this study for the investigation of the damaged skin tissues from mice models exposed to UV-B radiation and chemical cancer promoters. The main attraction of the Raman imaging technique is the possibility to obtain a „complete picture" the chemical species distribution in the very complex sample. Each Raman spectrum at a particular x-y coordinate contains a wealth of information about the chemical composition and molecular structure. For thin, dried tissue sections this technique is a powerful molecular imaging tool for detailed pathological assessment of the tissue. These images contain information about the molecular components and different components can be visualized by post-processing of data, because of the possibility of plotting the concentration (i.e. fingerprint band intensity) of various biochemicals as a function of position.

The aim of the Raman imaging was also to investigate whether the SERS effect can be applied to study tissue samples and further to probe the technique as a very sensitive tool for early cancer diagnostic. Tissue SERS was expected due to the colloidal silver nanoparticles in which the autopsy samples were immersed. Analyzing the samples using Raman spectroscopy, by acquiring single Raman spectra, we obtained either typical Raman signal characteristic for skin tissue supported by the literature, or different spectra with sharp bands, characteristic for SERS effect. One possible explanation for this could be the fact that the spectra were collected from regions where no silver nanoparticles penetrated the tissues. This is likely since the nanoparticles could not have been homogenously distributed within the tissue sample. As a general characteristic in the field of tissue SERS, the amide I band is less representative but in the Raman spectra it has significant intensity. This is first confirmation weather the spectra collected are Raman or SERS, along with the presence or absence of the huge Ag-molecule mode observed around 22o cm^{-1}[10-12]. When medium intensity contribution is observed, that would be a suggestion that pure Raman signal is also collected nearby the SERS from the microscope objective collection cone. This could have been possible because of inhomogeneity distribution of the Ag nanoparticles inside the tissue. Due tot his, the spot of the laser may have encompassed the margins of a "hot spot", meaning that the SERS enhancement conditions varied more in the distance and location of the target molecule relative to the enhancing silver nanoparticles.

RESULTS AND DISCUSSION

The first results after two weeks of the skin exposure to the UVB radiation (295 nm) and the chemical carcinogen (7,12-dimethylbenz(a) anthracene, DMBA) application indicated by skin redness, lesions and after one month of exposure the visual aspects pointed towards important skin damages like photo aging and first steps to skin carcinoma. To get a better insight on the nature of the damage and to detect the main molecular components in the samples, the histopathology results of the thin tissue sections were correlated with the spectroscopic data.

A specific area of 180x180 μm was chosen from the skin sample collected from the NMRI specimen. In Fig.1 the Raman image collected from the sample can be observed among with the microscopic picture of the entire sample and the area used for investigation (left). This region was selected based on the density of the tissue. The Raman image shown in the middle displays the distribution of the amide I band in the investigated tissue. The last image in Fig.1 represents the HCA result and the distribution of the three clusters obtained after the analysis. The black pixels represent spectra with negative Quality Test results, which were removed from the analysis. The spectra shown in the figure are color coded averaged spectra each corresponding to one of the three clusters.

The selected area was divided after the HCA analysis into three clusters. The green one, corresponding to the main part of the tissue, the red one which could be assigned to the margins of the tissue and the blue one which is observed only in a few scattered points on the image. Each of the spectra presented in Fig.1 are shown with the same color as the corresponding cluster. The spectra look rather similar, presenting the same main features, such as the 1447 cm^{-1} band assigned to CH_2 bending in proteins and lipids, 1343 and 1315 cm^{-1} bands specific for DNA, as well as collagen, in the case of the later, 1131 cm^{-1} band attributed to C-C stretching vibrations of lipids and C-N stretching vibrations of proteins, 1003 cm^{-1} characteristic to phenylalanine and the 854 cm^{-1} assigned to ring breathing of tyrosine and C-C stretching of hydroxyproline ring specific to collagen [16-18].

Though, at a closer look, slight differences between them can be seen. For example the two bottom spectra present the amide I band of collagen around 1670 cm^{-1}, absent in the upper one. On the other hand, spectrum number 1 corresponding to the blue cluster presents an intense band at 1577 cm^{-1} assigned to tryptophan protein and guanine and adenine nucleic acids. In the 1180-1340 cm^{-1} spectral range, the spectra present the same bands, though differently amplified. The most contributions seen here are proteins, amide III bands (1252, 1225 cm^{-1}), phenylalanine and tryptophan (1209 cm^{-1}), nucleic acids (1181 cm^{-1}) and collagen (1316 cm^{-1}) [16-18]. Another

difference lies in the band seen at 477 cm^{-1}, which has a very weak intensity in the green spectrum compared to the other two. Also, the 322 cm^{-1} seen more amplified in the bottom spectrum is assigned to the substrate of CaF_2 on which the thin tissue sections were placed.

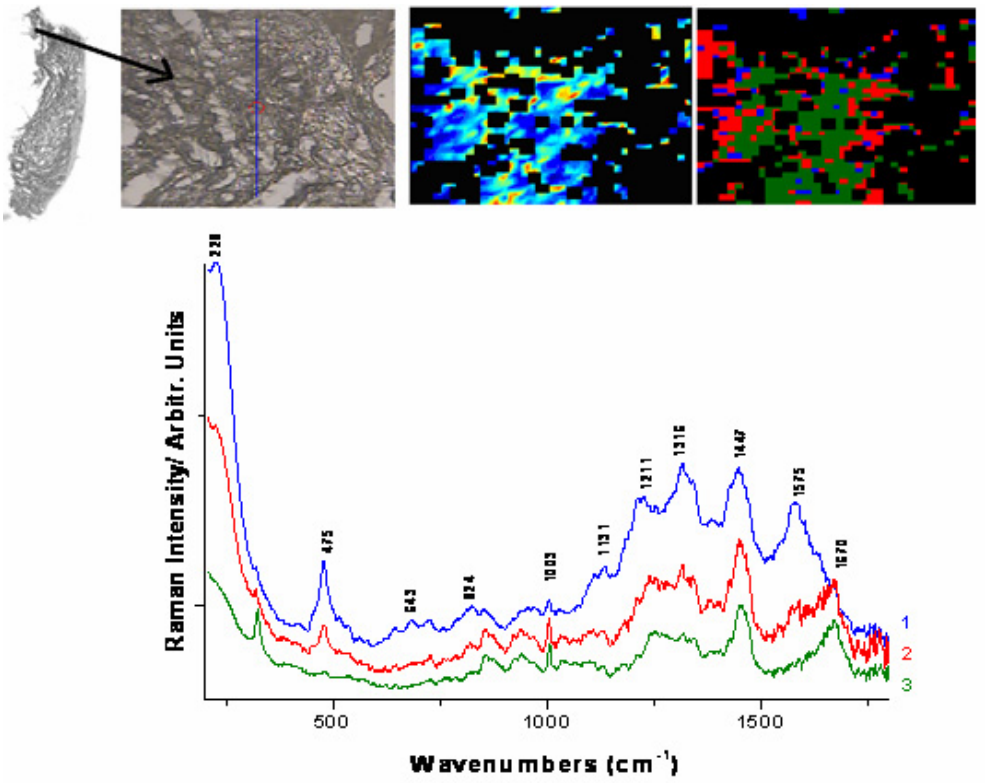

Figure 1. Microscopic image of the NMRI skin sample and the image of the area selected for investigation, the Raman map and the three clusters resulted after HCA analysis. In the below image the averaged-clustered spectra are presented, each corresponding to one cluster

One important observation is the appearance of the band at 228 cm^{-1} in the upper spectrum. This band can be seen in the middle one as well, though it seems as if it is not complete. The band could indicate the formation of Ag-O bond, meaning that the silver nanoparticles have penetrated the tissue and attached to the target molecules (SERS fingerprint). This could suggest that the upper spectrum is a SERS one, implying the method used in this study for acquiring SERS signal from biological tissues by inoculating them into colloidal nanoparticles, succeeded.

Keeping this in mind, an obvious conclusion would be that the only true SERS spectrum is the upper one assigned to the blue scattered cluster in the HCA image. The middle spectrum assigned to the red cluster has both Raman and SERS contributions and could be a result of the fact that the focus of the laser could have encompassed the margins of a “hot spot”, meaning that the SERS enhancement conditions varied more in the distance and location of the target molecule relative to the enhancing silver nanoparticles. Another aspect that needs to be pointed out is the fact that the Ag nanoparticles are not distributed homogenously inside the tissue. The lower spectrum assigned to the main part of the tissue, the green cluster, is a Raman spectrum being very similar to the single Raman spectra acquired from the same sample (not shown here).

Analyzing the entire Raman image, SERS variability became evident in many ways. The intensity of the acquired signals varied from one point of acquisition to another and the resulted signals showed differences in peak locations. To understand what happened inside the tissue with the Ag colloidal nanoparticles, in Fig. 2 are presented three spectra found in the Raman image acquired from three consecutive points.

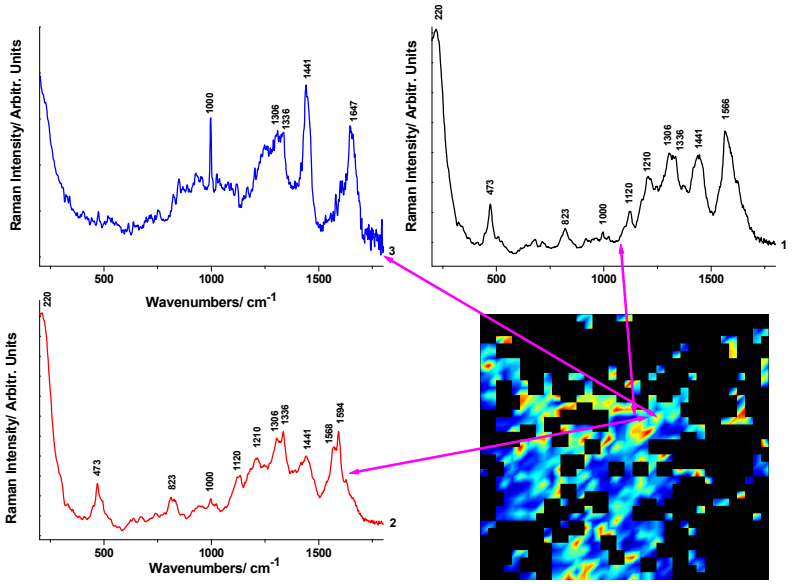

Figure 2. SERS spectra (1 and 2) in comparison to a Raman spectrum (3) acquired from three consecutive points from the Raman image.

Spectra 1 and 2 are SERS spectra, while the third is a Raman one. The differences between the Raman and the SERS spectra can easily be noticed, such as the absence of the amide I band at 1647 cm^{-1} from the SERS spectra, or the sharp intense phenylalanine band at 1000 cm^{-1} seen in the Raman spectrum.

On the other hand both SERS spectra present the 1568 cm^{-1} band assigned to tryptophan and nucleic acids [14], the 1210 cm^{-1} band assigned to phenylalanine and tryptophan [12], the 1120 cm^{-1} attributed to C-N stretching of proteins and C-C stretching of lipids and the 820 cm^{-1} band assigned to out of plane ring breathing of tyrosine and O-P-O stretching vibrations of DNA [12]. Although the main bands can be seen at the same wavenumbers, they are differently amplified and other weaker signals can be spotted as well. One possible explanation for the observed differences in the SERS spectra could be the fact that certain frequencies of scattering are more sensitive to the enhancement than others. Additionally, different portions of the tissue could have been subjected to the enhancement during the measurement. Depending on how many adsorbed molecules on the Ag nanoparticles, does the spot of the laser encompass, the spectra can present lots of fluctuations in signal intensities and frequencies. However, the epithelial layer would be more suitable for such SERS sensitive characterization and consequently, the method support further optimizations concerning the Ag nanoparticles incubation in order to perform routine applications in skin tissue monitoring.

For the present study we employed the damaged skin tissue only. Obviously, further SERS studies are required in order to investigate the molecular spectral response from normal tissue specimens for establishing an appropriate differentiation algorithm for early diagnostic.

CONCLUSIONS

In this study we have applied Raman imaging technique in conjunction with the SERS effect for the investigation of in vivo damaged biological skin tissues from mice specimens. The imaging display was obtained using the amide I band from proteins characteristic for tissue. SERS effect was evidenced for the studied skin sample. By inoculating Ag colloidal nanoparticles in biological tissues, we have proved here the possibility of recording SERS spectra which can be used to investigate the nature of the molecular components of carcinogenic skin tissue samples. To the best of our knowledge this is the first time when SERS effect was detected from skin tissues prepared in this manner.

EXPERIMENTAL SECTION

Sample Preparation and Animals Protocol: Female mice (NMRI specimens, 8 weeks old) were purchased from Charles River. The UMFT Bioethical Committee agrees the protocol and institutional guidelines were followed in the handling and care the animals. For the present study 2 animals from a group of 10 mice that were treated for skin carcinoma development were chose. The animals were accommodated to UMFT Biobase and they have been maintained in optimal conditions. The food was standard and was administrated as the water *ad libitum*. The day/night cycle was 12/12 hours and the humidity over 55%.

Tumor induction protocol has been largely described elsewhere [13,14]. For this study, NMRI mice specimens were exposed daily to UV radiation (295 nm) and orally in one dose completed by locally treated with 7,12-dimethylbenz(a)anthracene (DMBA) solution, a synthetic polycyclic aromatic hydrocarbon known to induce cancer in different organs. The skin carcinoma experimental model has been investigated after 10 weeks of photo-chemical damage evolution. Tissue samples were collected from the sacrificed mouse by CO_2 inhalation. For the skin biopsy only they were anesthesied with xylazine and ketamine. Samples from the skin were detached and immersed in 10% formalin solution mixed with colloidal silver nanoparticles prepared according to the Lee Meisel method. From these samples, thin tissue sections were prepared using a LEICA CM3050S cryostat and placed on CaF_2. The samples were not submitted to any preparation, like “freezing shock” in liquid nitrogen or washing.

Instrumentation: The Raman maps were collected using a Raman microscope coupled to a 785 nm diode laser (Kaiser Optical Systems). Each map had a dimension of 19 x 19 =361 spectra with a step size of 10 μm, exposure time 2 s per spectrum, number of acquisitions 2 and dwell time between 10-30 s. The laser power was set to 200 mW.

Data analysis: The resulting Raman images were processed using the CytoSpec [15] software package. The data sets were normalized resulting in a linear correction of the complete spectrum, removing all negative intensities, background subtraction, polynomial baseline correction and filtering. Low-intensity spectra were removed from the data sets because they corresponded to positions outside the tissue, near holes, near fissures or near margins. The intensity of the amide I band at 1656 cm^{-1} was used to determine whether some regions of the sample were too thin for the spectra to be included in the subsequent data analysis. In the end clustering analysis was performed on the data sets.

Cluster analysis identifies regions of the sample that have similar spectral response by clustering the spectra into groups or clusters such that differences in the intra-cluster spectral responses are minimized while simultaneously maximizing the inter-cluster differences between spectral responses. The hierarchical cluster analysis (HCA) algorithm calculates the symmetric distance matrix (size n×n) between all considered spectra (number n) as a measure of their pair wise similarity. The algorithm then searches for the minimum distance, collects the two most similar spectra into a first cluster and recalculates spectral distances between all remaining spectra and the first cluster. In the next step the algorithm performs a new search for the most similar objects, which now can be spectra or clusters. The two most similar objects are clustered again and the distance values of the newly formed cluster are recalculated. This iterative procedure is repeated n−1 times until all spectra have been merged into one cluster.

ACKNOWLEDGMENTS

This work was supported by CNCSIS-UEFISCSU grants (PNII-IDEI code 2284/2008 and 1257/2007). A. Falamas thanks to Dr. Christoph Krafft and Professor Jürgen Popp ("Friedrich Schiller" University of Jena, Germany) for useful discussions and access to laboratory facilities.

REFERENCES

1. C. Kendall, M. Isabelle, F. BayabtßHegemark, J. Hutchings, L. Orr, J. Babrah, R. Baker, N. Stone, *Analyst*, **2009**, *134*, 1029.
2. Ch. Krafft, B. Dietyek, J. Popp, *Analyst*, **2009**, *134*, 1046.
3. Ch. Krafft, M. Kirsch, C. Beleites, G. Schackert, R. Salzer, *Anal. Bioanal. Chem*., **2007**, *389*, 1133.
4. M. Schmitt, J. Popp, *J. Raman Spectrosc.*, **2006**, *37*, 20.
5. K. Hering, D. Cialla, D. Ackermann, K. Doerfer, T. Meolleer, R.H. Scheidewind, R. Mattheis, W.R. Fritysche, P. Roesch, J. Popp, *Anal. Bioanal. Chem.*, **2008**, *390(1),* 113.
6. M. Fleischmann, P.J. Hendra, A.J. Mcquillian, *Chem. Phys. Lett*., **1974**, *26*, 123.
7. D.L. Jeanmarie, R.P. Van Duyne, *J. Electroanal. Chem.*, **1977**, *84*, 1.
8. M.G. Albrecht, J.A. Creighton, *J. Electroanal. Chem.*, **1977**, *99(15),* 5215.
9. M. Moskovits, , *Rev. Mod. Phys.*, **1985**, *57(3),* 783.
10. S. Cinta Pinzaru, L.M. Andronie, I. Domsa, O. Cozar, S. Astilean, *J. Raman Spectrosc.*, **2008**, *39*, 331.

11. X. Qian, X.H. Peng, D.O. Ansari, Q. Yina-Goen, G.Z. Chen, D.M. Shin, L. Yang, A.N. Young, D. May, M.D. Wang, S. Nie, *Nat. Biotechnol.*, **2008**, *26*, 83.
12. S. Fendel, B. Schrader, *Fresenius J. Anal. Chem.,* **1998**, *360*, 609.
13. C. Dwivedi, E.R. Maydew, J.J. Hora, D.M. Ramaeker, X. Guan, *Eur. J. Cancer Prev.,* **2005**, *14(5),* 473.
14. L.H. Kligman, R. Elenitsas, *Melanoma Res.*, **2001**, *11*, 319.
15. *CytoSpec - Application for FT-IR spectroscopy imaging*, www.cytospec.com.
16. R.E. Kast, G.K. Serhatkulu, A. Cao, A.K. Pandya, H. Dai, J.S. Thakur, V.M. Naik, R. Naik, M.D. Klein, G.W. Aunner, R. Rabah, *Biopolym.* (*Biospectrosc.*), **2008**, *89(3),* 235.
17. M.V.P. Chowdary, K.K. Kumar, S. Mathew, L. Rao, C.M. Krishna, J. Kurien, *Biopolym.* (*Biospectrosc.*), **2009**, *91(7),* 539.
18. I. Nottingher, S. Verrier, S. Haque, J.M. Polak, L. Hench, *Biopolym.* (*Biospectrosc.*), **2003**, *72*, 230.